Thin-Walled Structures 78 (2014) 70–78

Contents lists available at ScienceDirect

Thin-Walled Structures

journal homepage: www.elsevier.com/locate/tws

Experimental and numerical studies on the quasi-static and dynamic crushing responses of multi-layer trapezoidal aluminum corrugated sandwiches

Cenk Kılıçaslan [a,b], Mustafa Güden [a,b,*], İsmet Kutlay Odacı [a,b], Alper Taşdemirci [a,b]

[a] Dynamic Testing and Modeling Laboratory, Izmir Institute of Technology, Gülbahçe Köyü, Urla, Izmir, Turkey
[b] Department of Mechanical Engineering, Izmir Institute of Technology, Gülbahçe Köyü, Urla, Izmir, Turkey

ARTICLE INFO

Article history:
Received 16 May 2013
Received in revised form
11 November 2013
Accepted 17 January 2014

Keywords:
Corrugated
Compression
Simulation
Multilayer
Sandwich

ABSTRACT

The axial crushing responses of bonded and brazed multi-layer 1050 H14 trapezoidal aluminum corrugated core (fin) sandwich structures, with and without aluminum interlayer sheets in 0°/0° and 0°/90° core orientations, were both experimentally and numerically investigated at quasi-static and dynamic strain rates. Multi-layering the core layers decreased the buckling stress and increased the densification strain. The experimental and simulation compression stress–strain curves showed reasonable agreements with each other. Two main crushing modes were observed experimentally and numerically: the progressive fin folding and the shearing interlayer aluminum sheets. Both, the simulation and experimental buckling and post-buckling stresses increased when the interlayer sheets were constraint laterally. The multi-layer samples without interlayer sheets in 0°/90° core orientation exhibited higher buckling stresses than the samples in 0°/0° core orientation. The increased buckling stress of 0°/0° oriented core samples without interlayer sheets at high strain rate was attributed to the micro-inertial effects which led to increased bending forces at higher impact velocities.

1. Introduction

Sandwich structures are the structural components which are conventionally used in diverse structural applications. The main advantage in using these structures is derived from the relatively high strength to weight ratios combined with the relatively high energy absorption capabilities. A variety of metallic core materials have been subjected to experimental and numerical investigations, particularly aiming to improve the impact resistance of sandwich structures, including aluminum foams [1–9] and honeycombs [10–15]. Corrugated structures have been developed as light-weight core materials, providing light-weight and high crushing strength to the sandwich structures as similar with foams and honeycombs. Corrugated structures are manufactured easily into intricate geometries and have homogeneous macro-structure [16]. There have been apparently numerous experimental and numerical investigations and reviews in the literature on the quasi-static/dynamic mechanical and impact/blast loading responses of sandwich structures with periodic cellular metal cores, including honeycomb, corrugated and lattice truss topologies, for example see the review by Wadley in 2006 [17]. The most widely investigated topologies include V-type [18,19], U-type [20,21], X-type (diamond) [22] and Y-type [19,23,24] corrugated and pyramidal truss [16,25,26] structures. The previous experimental and accompanying numerical investigations were on the single layer corrugations; while, the effect of layering on the overall performance of multi-layer corrugated metal core sandwiches has not been investigated. In this study, the crushing responses of multi-layer 1050 H14 trapezoidal aluminum corrugated core sandwich structures were determined at quasi-static (10^{-3} and $10^{-1}\,s^{-1}$) and dynamic strain rates ($40\,s^{-1}$), both experimentally and numerically. In the previous studies, comparative studies were performed on the indentation and projectile impact behavior of layered corrugated aluminum and aluminum foam core sandwich panels [5,27]. This study is an extension of the pervious study and aims at determining and modeling the quasi-static and dynamic compression deformation behavior of multi-layer trapezoidal aluminum corrugated sandwiches. The comparisons between the mechanical responses of single- and multi-layer corrugated structures with and without aluminum sheet interlayers in two different core orientations were also presented. The effects of sandwich specimen assemble methods, namely adhesive bonding and brazing, on the crushing response were also assessed.

2. Sandwich structure construction

Multi-layer corrugated core sandwich structures were constructed by sequentially assembling 1050 H14 aluminum trapezoidal

* Corresponding author at: Dynamic Testing and Modeling Laboratory, Izmir Institute of Technology, Gülbahçe Köyü, Urla, Izmir, Turkey. Tel.: +90 232 7506001; fax: +90 232 7506701.
E-mail address: mustafaguden@iyte.edu.tr (M. Güden).

0263-8231/$ - see front matter © 2014 Elsevier Ltd. All rights reserved.
http://dx.doi.org/10.1016/j.tws.2014.01.017

zig-zag corrugated aluminum fin layers (Fig. 1(a)), aluminum interlayer sheets and aluminum face sheets. The height, width and thickness of the fins in the corrugated aluminum layer are sequentially 9, 5 and 0.135 mm as shown in Fig. 1(b). The core layers are commercially produced by a local factory using a sheet metal forming press in the specified fin geometry for the heat exchangers. The zig-zag form of fins improves the heat conduction between layers. The thicknesses of aluminum interlayer sheets and face sheets were 0.5 mm and 1.5 mm, respectively.

The tested multi-layer corrugated core sandwich specimens consist of bonded/brazed seven corrugated fin layers in 0°/0° orientation, six interlayer sheets and two face sheets (Fig. 2(a) and (b)). The bonded panels were assembled using a Henkel Thomsit R710 polyurethane adhesive. Sandwich samples were also assembled through brazing in order to assess the effect of brazing on the crushing behavior. The brazing process was performed by the corrugated fin producer at 600 °C for 10 min under atmospheric pressure following the surface cleaning and flux slurry spraying. An aluminum 4343 alloy sheet was used as filler between layers with an amount of about 7 wt%. Multi-layer samples without interlayer sheet in 0°/0° and 0°/90° fin layer orientations were prepared using adhesive bonding (Fig. 2(c)). Single-layer sandwiches composing of a fin layer and two face sheets were prepared using the same adhesive and tested for comparison. The density of multi-layer corrugated sandwiches with interlayer sheets varies with the number of fin layers as shown in Fig. 3. The density of adhesively bonded sandwiches reaches almost a constant value of 0.35 g cm^{-3} after about 20 fin layers. The use of adhesive increases the density of multi-layer corrugated sandwich by 0.05 g cm^{-3}. The densities of tested brazed and polyurethane bonded sandwiches with interlayers were similar; ~0.39 g cm^{-3}, while the sandwiches without bonding layer were ~0.36 g cm^{-3}. The density of the corrugated fin layers without interlayer sheets was 0.115 g cm^{-3}, corresponding to a relative density of 0.042.

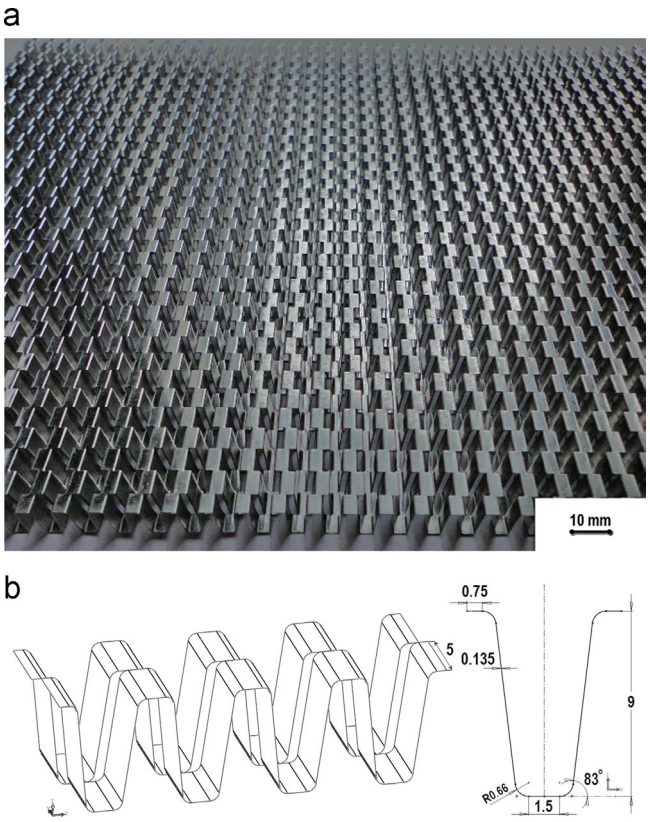

Fig. 1. (a) The picture of a corrugated fin layer and (b) isometric view and geometric variables of corrugated fin.

3. Experimental methodology

The quasi-static tensile stress–strain curves of 1050 H14 aluminum were determined at the strain rate of 10^{-3} s^{-1}. The test specimens were machined in accord with ASTM E 8M-04 Standard [28]. The gage length and thickness were 60 and 1.5 mm, respectively. The displacements of test specimens were recorded using a video extensometer. The stress–strain behavior of 1050 H14 alloy after brazing was determined by testing the heat-treated tensile test specimens. These samples were heat treated at 600 °C for 10 min with the same heating and cooling rates applied in the brazing process.

The quasi-static compression tests on the adhesively bonded and brazed rectangular sandwich specimens ($50 \times 50 \times 70$ mm^3) were conducted at 10^{-3} and 10^{-1} s^{-1}. The dynamic compression tests (40 s^{-1}) on the adhesively bonded and brazed rectangular sandwich specimens were performed in a FRACTOVIS drop weight tower. The main parts of the drop weight tower test machine, striker, platen, photocells and the bottom plate, are shown in Fig. 4(a). The striker was attached to a 45 kN piezoelectric force transducer. The striker velocity was measured by the photocells of drop weight tower. In a typical test, the specimen was placed on the bottom plate and the striker with an initially attained velocity crushed the specimen. The total mass of impact system

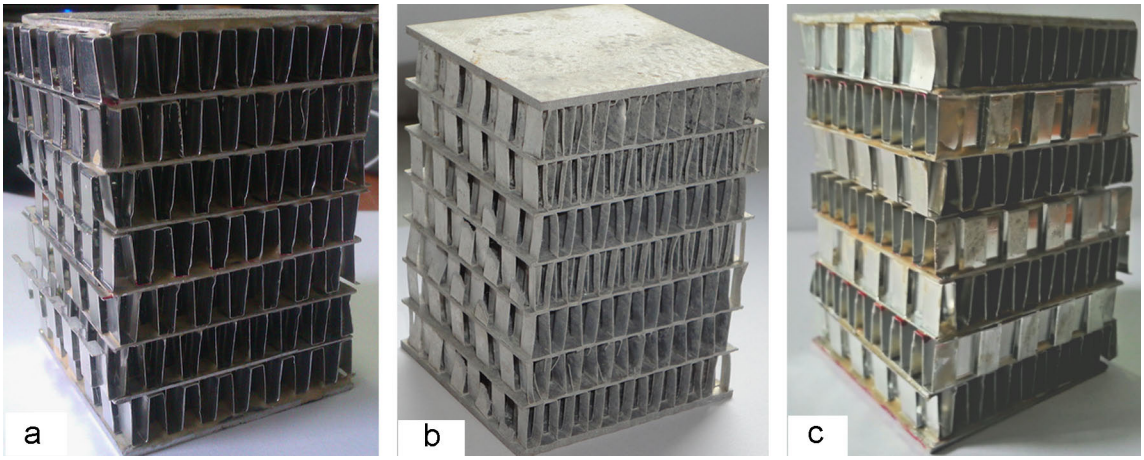

Fig. 2. Multi-layer corrugated sandwich specimens: (a) bonded 0°/0° oriented; (b) brazed 0°/0° oriented and (c) bonded 0°/90° oriented.

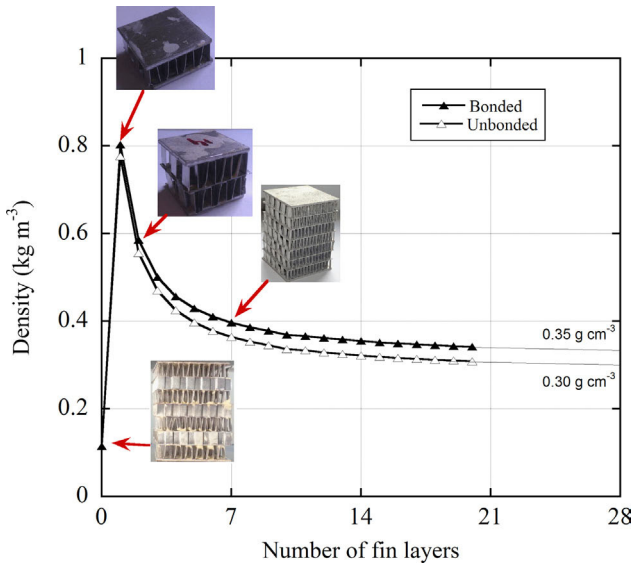

Fig. 3. Density vs. number of fin layers of bonded and unbounded single- and multi-layer sandwiches.

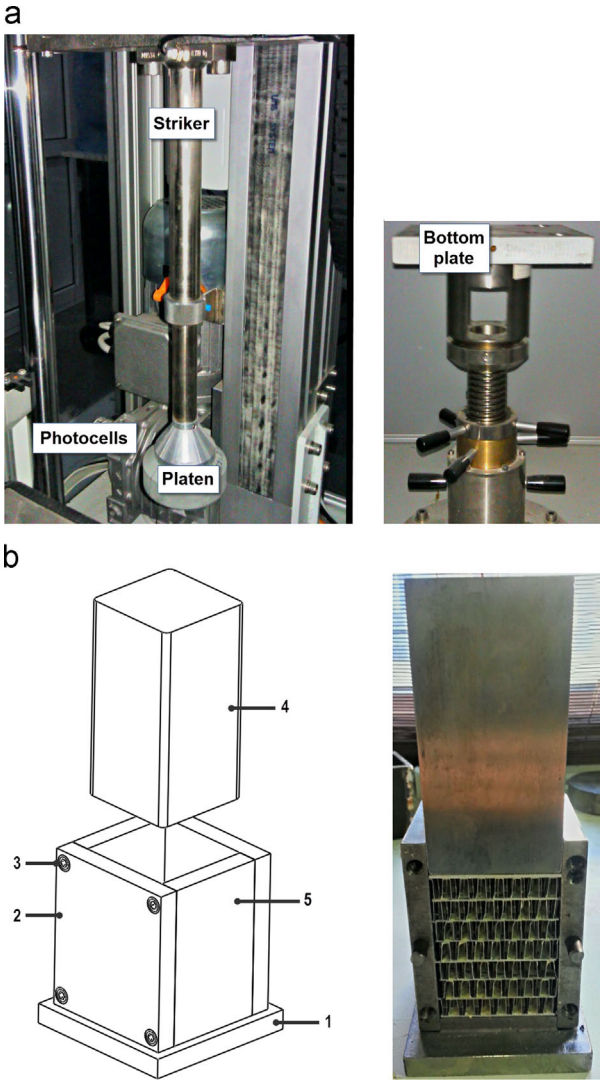

Fig. 4. (a) Drop weight tower test machine and its components and (b) constraint compression test die.

was 15.778 kg. The tests were performed at 3 m s^{-1} using a flat-end striker. The diameter of the striker end was 70 mm. The deformations of test samples were recorded using a high speed camera (Fastcam Photron) with the frame rate of 5000 fps (frame per second). In parallel, the constraint compression tests were performed at the strain rate of 10^{-1} s^{-1} using a rectangular screwed closed-die shown in Fig. 4(b). The sandwich specimen was placed inside the die and with a punch (Part no. 5 in Fig. 4(b)) the specimen was axially compressed in the die. In order to reduce the friction between the die and test sample, the surfaces of the die were lubricated using grease.

4. Numerical modeling

Full geometrical model simulations of quasi-static and dynamic tests were implemented in the non-linear explicit finite element code of LS-DYNA [29]. The finite element models of 0°/0° fin layer orientated sandwich sample with interlayer sheets and 0°/0° and 0°/90° fin layer orientated samples without interlayer sheets are sequentially shown in Fig. 5(a)–(c). Trapezoidal corrugated fin layers were meshed using Belytschko–Tsay shell elements with five integration points and the interlayer and face sheets were modeled using constant stress solid elements. The increased number of integration points in shell elements raise the CPU calculation times. In case buckling is the dominant deformation mode; however, the number of integration points should be higher than two in order to increase the accuracy of the models [30]. The finite element meshes of corrugated fin layers and interlayer/face sheets have to coincide with each other in order to define tied contacts between them. This limits the implementations of arbitrary-defined mesh distribution and element sizes.

MAT_SIMPLIFIED_JOHNSON_COOK material model, material type 98, was used to model 1050 H14 aluminum alloy. Johnson and Cook (JC) flow stress model is given as [31],

$$\sigma = [A + B\varepsilon^n]\left[1 + c\ln\left(\frac{\dot{\varepsilon}}{\dot{\varepsilon}_0}\right)\right][1 - (T^*)^m] \quad (1)$$

where σ, ε, $\dot{\varepsilon}$ and $\dot{\varepsilon}_0$ are, respectively, the effective plastic strain, strain rate, and reference strain rate; A, B, n, c, and m are the model parameters. The last term T^* is expressed as

$$T^* = \frac{T - T_r}{T_m - T_r} \quad (2)$$

where T is the temperature and T_r and T_m are the reference and melting temperatures, respectively. Material type 98 does not take into account temperature effect, the last bracket of Eq. (1). As aluminum alloys have no or negligible strain rate dependent flow stress; the second brackets of Eq. (1) is also omitted in the material model. The model parameter A stands for the yield strength, B for the strengthening by strain hardening and n for the strain hardening. In order to determine the model parameters, at least 3 tension tests were performed at the quasi-static strain rate. An average true stress–true plastic strain curve was then constructed from these tests. The model parameters were then determined through fitting Eq. (1) to the average true stress–true plastic strain curve. The contacts between core, interlayer and face sheets were assumed to be perfectly bonded and defined by TIED_NODES_TO_SURFACE contact algorithm. The self-contacting interfaces were defined by ERODING_SINGLE_SURFACE contact type.

The developed full numerical models of quasi-static compression test system and drop weight test are shown in Fig. 6((a) and (b)), respectively. The numerical model of quasi-static compression test comprised of top and bottom compression test platens and the specimen. Each platen model consisted of 19,200 constant stress solid elements. Quasi-static simulations were performed at

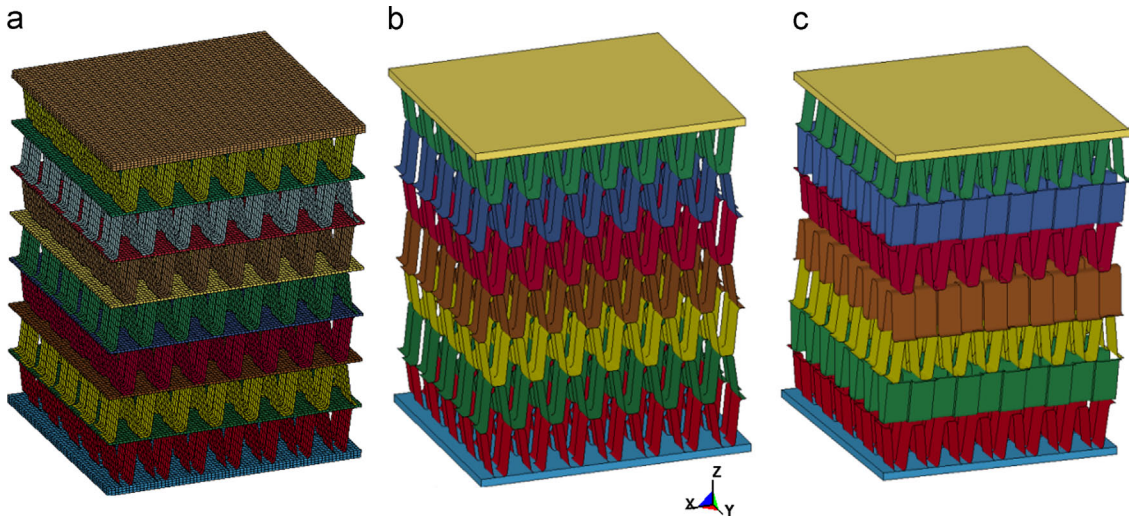

Fig. 5. Numerical models of (a) 0°/0° core oriented sandwich and (b) 0°/0° and (c) 0°/90° core oriented sandwiches without interlayer sheets.

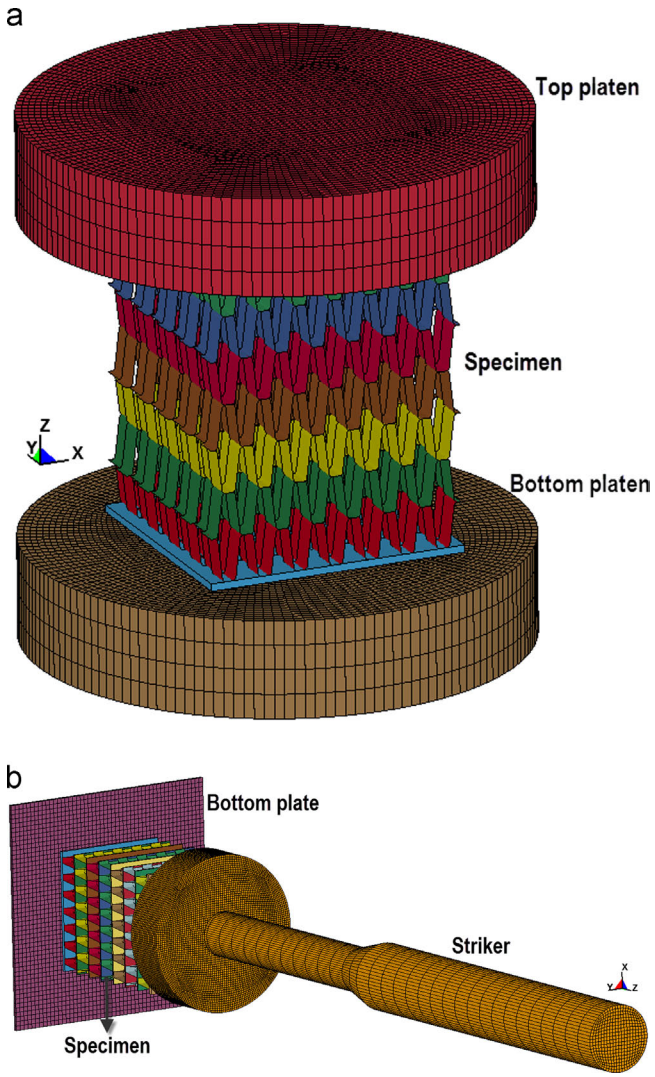

Fig. 6. (a) Quasi-static compression and (b) drop weight tower test numerical models.

the strain rate of $10^{-1}\,s^{-1}$ in order to reduce CPU time. The flat-end of the striker, which was in direct contact with specimen, was meshed using 1 mm, while the rest was modeled using 10 mm

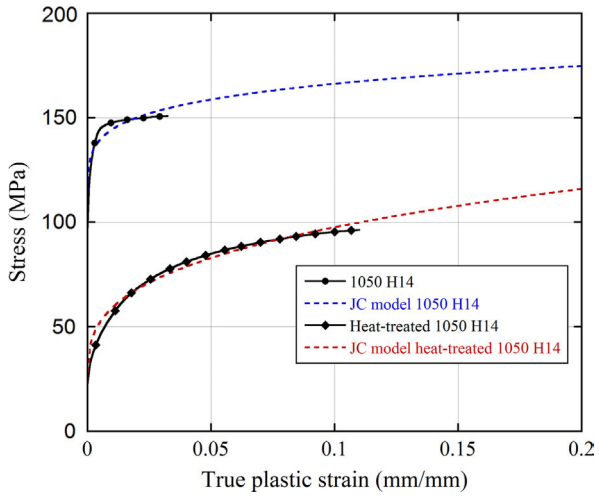

Fig. 7. Experimental and JC model true stress vs. true plastic strain curves of 1050 H14 Al alloy.

element sizes. The striker was defined to move only in the *z*-direction and consisted of 106,192 constant stress solid elements. The stationary bottom plate model comprised 5000 solid quad elements. The contact between the cross-head and the specimen was defined by AUTOMATIC_SURFACE_TO_SURFACE contact. The static and dynamic friction coefficients were set to 0.3 and 0.2, respectively. Similar to the drop weight experiments, the initial velocity of the striker in the model was set to $3\,m\,s^{-1}$. In quasi-static simulations, the mass scaling was applied by defining a positive time step value in CONTROL_TIMESTEP card in LS-DYNA.

5. Results and discussions

The experimental and JC model true stress–true plastic strain curves of 1050 H14 and heat-treated 1050 Al alloys are shown in Fig. 7. The yield stresses of as-received and heat-treated 1050 Al alloy are 102 MPa and 24 MPa, respectively. The JC model parameters were determined by fitting the first bracket of Eq. (1) with the experimental true stress–true plastic strain curves. The experimental curves were determined as the average of three tests. The determined JC parameters of as-received and heat-treated Al alloys are tabulated in Table 1. The JC model true stress–true

plastic strain curves agree well with those of experiments as shown in Fig. 7.

The stress–strain curves of single- and multi-layer specimens ($50 \times 50 \times 70\ mm^3$) tested at the strain rate of $10^{-3}\ s^{-1}$ and the multi-layer specimens tested at the strain rates of $10^{-3}\ s^{-1}$ and $40\ s^{-1}$ are shown in Fig. 8(a). The deformation sequence pictures of multi-layer sandwiches tested at $10^{-3}\ s^{-1}$ and $40\ s^{-1}$ are further shown at various strain levels in Fig. 8(b) and (c), respectively. The buckling stresses of three tests of single-layer specimens at $10^{-3}\ s^{-1}$ varied between 0.73 and 0.91 MPa. The bucking stress (initial peak stress) of the multi-layer samples tested at quasi-static strain rates vary between 0.45 and 0.6 MPa. Multi-layering; therefore, decreases the buckling stress below that of single-layer. The stress–strain behavior of the multi-layer samples tested at $40\ s^{-1}$; however, shows increased buckling stress (~0.75 MPa), while the post-buckling stress levels are very much similar with those of the quasi-statically tested multi-layer samples. The collapse begins with the buckling of a fin layer at one of the ends of the specimen accompanied by the interlayer sheet shearing (Fig. 8(b) and (c)). The prescribed deformation mode is progressive until all the layers collapse (0.7 strains). The densification strain is noted to increase from ~0.6 in single-layer to ~0.7 in multi-layer configuration. Since, there are seven corrugated layers; the seven peak stresses in the stress–strain curves will correspond to the collapse of individual layers. The missing peak stresses in the curves of Fig. 8(a) are attributed to the collapse of two or more corrugated layers concurrently. As noted in Fig. 8(a), after the densification strain of ~0.7, the deformation proceeds with the compression of folded layers and face sheets altogether, leading to abrupt increase in stress values. This deformation type is analogous to elastic–plastic metal foam deformation behavior in the densification region [32]. The deformation modes of brazed corrugated multi-layer samples are pretty much similar with those of bonded samples, but the crushing stresses are 3–4 times lower at the same strain rates (Fig. 9). As similar with the bonded samples, the brazed samples show an increased buckling stress (0.2 MPa) at $40\ s^{-1}$ as compared with quasi-static test (0.16 MPa) as seen in Fig. 9. A higher number of the occurrences of the

Table 1
JC model parameters of 1050 H14 Al alloy.

Material	A (MPa)	B (MPa)	n	ε_f
1050 H14 Al	102	97.252	0.18	0.62
1050 H14 Al (heat-treated)	24	154.27	0.32128	0.8646

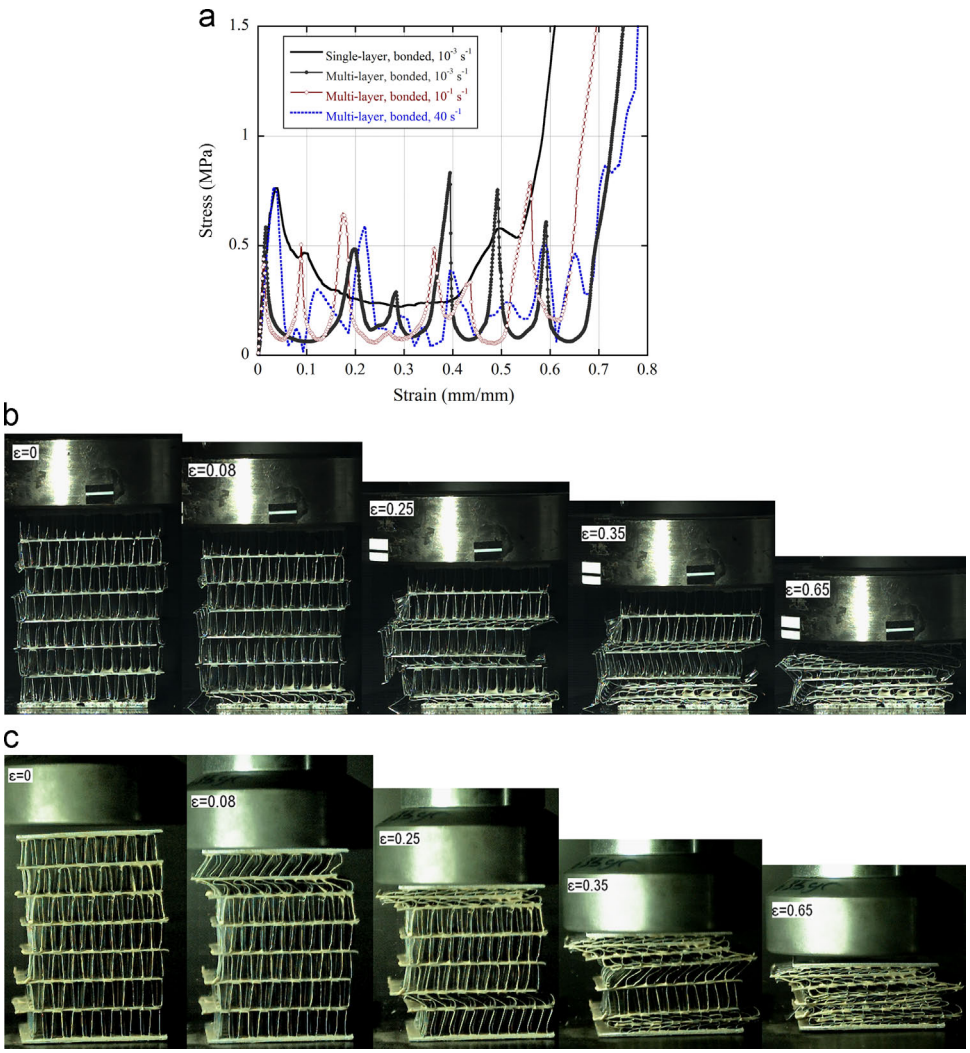

Fig. 8. (a) Stress–strain curves of single- and multi-layer sandwich specimens tested at the strain rate of $10^{-3}\ s^{-1}$ and multi-layer sandwich specimens tested at the strain rates of 10^{-3}, 10^{-1} and $40\ s^{-1}$ and the deformation steps of bonded multi-layer sandwich specimens at the strain rate of (b) $10^{-3}\ s^{-1}$ and (c) $40\ s^{-1}$.

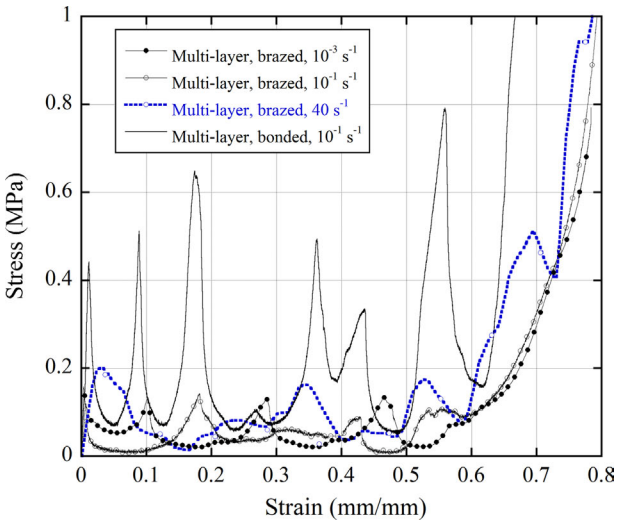

Fig. 9. Stress–strain curves of bonded multi-layer sandwich specimens tested at the strain rate of 10^{-3} and 40 s^{-1} and brazed multi-layer sandwich specimens tested at the strain rates of 10^{-3}, 10^{-1} and 40 s^{-1}.

concurrent collapse of corrugated layers were also observed in the brazed samples. This behavior is also reflected in the stress–strain curves of Fig. 9 with the higher number of missing peak stresses.

The experimental and simulation unconstraint and constraint tests stress–strain curves of bonded samples at the strain rate of 10^{-1} s^{-1} are shown in Fig. 10(a) and (b), respectively. In the same figures, the corresponding average stresses are also drawn for comparison. The simulation unconstraint test yields higher crushing stresses than the experiment until about 0.2 strains; but the difference vanishes at increasing strain levels. The experimental buckling and average stresses for unconstraint tests are 0.45 and 0.16 MPa, respectively. Both, the experimental and simulation deformation modes of unconstraint samples are very much similar, consisting of fin wall buckling and interlayer sheet shearing (the inset of Fig. 10(a)). The sheared layers are squashed to the sides of the sample after the deformation. Both, simulation and experimental buckling and post bucking stresses increase in constraint tests as shown in Fig. 10(b). The buckling and average stresses of constraint samples are 0.62 and 0.38 MPa, respectively. If one considers the post-buckling stress as the plateau stress, it may be concluded that the constraining reduces the differences between buckling and plateau stress. The deformation in constraint tests proceeds more homogeneously: 7 peak stresses occur at the beginning of the buckling of each corrugated layer. The constraint specimen is noted to experience merely fin wall folding and show no squash through sides (the inset of Fig. 10(b)). It is concluded that the major effect of constraining is on the post-buckling stresses (average stress); while the buckling stress is less affected by constraining.

The compression experimental and simulation stress–strain curves of unconstraint bonded and brazed samples at 40 s^{-1} are shown together in Fig. 11(a). The simulation buckling and post buckling stresses are very similar with the experimental buckling and post buckling stresses; while bonded samples show higher crushing stresses than brazed samples at 40 s^{-1}, as similar with quasi-static loading. The numerical dynamic buckling stresses of bonded and brazed samples are sequentially 0.68 and 0.25 MPa and the corresponding experimental values are 0.75 and 0.2 MPa, respectively. The dynamic constraint tests stress–strain curves of bonded and brazed samples are shown in Fig. 11(b). In the same figure the quasi-static stress–strain curve of bonded samples are also shown for comparison. The constraint tests at dynamic strain rate show the similar buckling stresses with the unconstraint tests

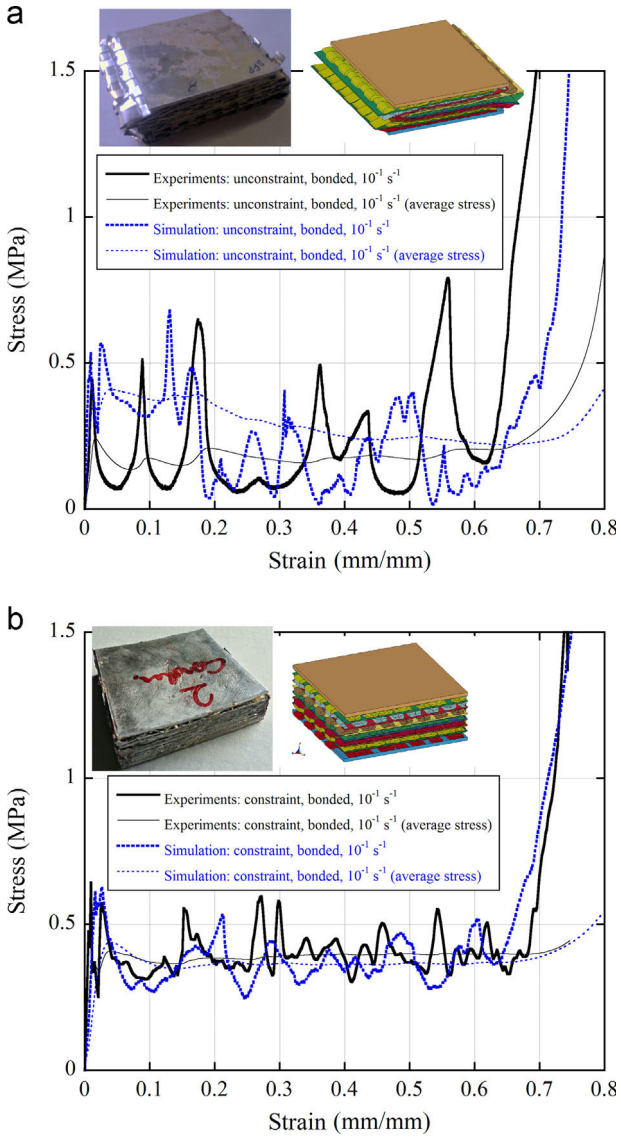

Fig. 10. Simulation and experimental stress–strain curves and final deformed shapes of bonded multi-layer sandwiches tested at 10^{-1} s^{-1}: (a) unconstraint and (b) constraint tests.

but again the post buckling stresses increase with constraining. The average crushing stress is ~0.38 MPa for bonded and ~0.18 MPa for brazed samples. It is also noted that the increasing strain rate has no significant effect on the buckling and post buckling stresses of bonded constraint samples. The deformation sequences of the unconstraint test simulation and experiment show close resemblances as depicted in Fig. 11(c) and proceed with the fin wall buckling and interlayer sheet shearing.

The effect of corrugation layer orientation (0°/0° and 0°/90°) on the stress–strain and average stress–strain curves of bonded multi-layer sandwich samples are shown in Fig. 12. The samples with 0°/90° core orientation show higher buckling stress than the samples with 0°/0° core orientation. However, the core orientation has almost no effect on the average stress of bonded sandwich samples.

The experimental and simulation compression stress–strain curves and deformation pictures of the bonded 0°/0° and 0°/90° core oriented multi-layer specimens without interlayer sheets at the strain rate of 10^{-1} s^{-1} are shown in Fig. 13(a) and (b), respectively. As seen in Fig. 13(a), in the absence of interlayer sheets, the fins opens laterally, leading to shearing type non-progressive

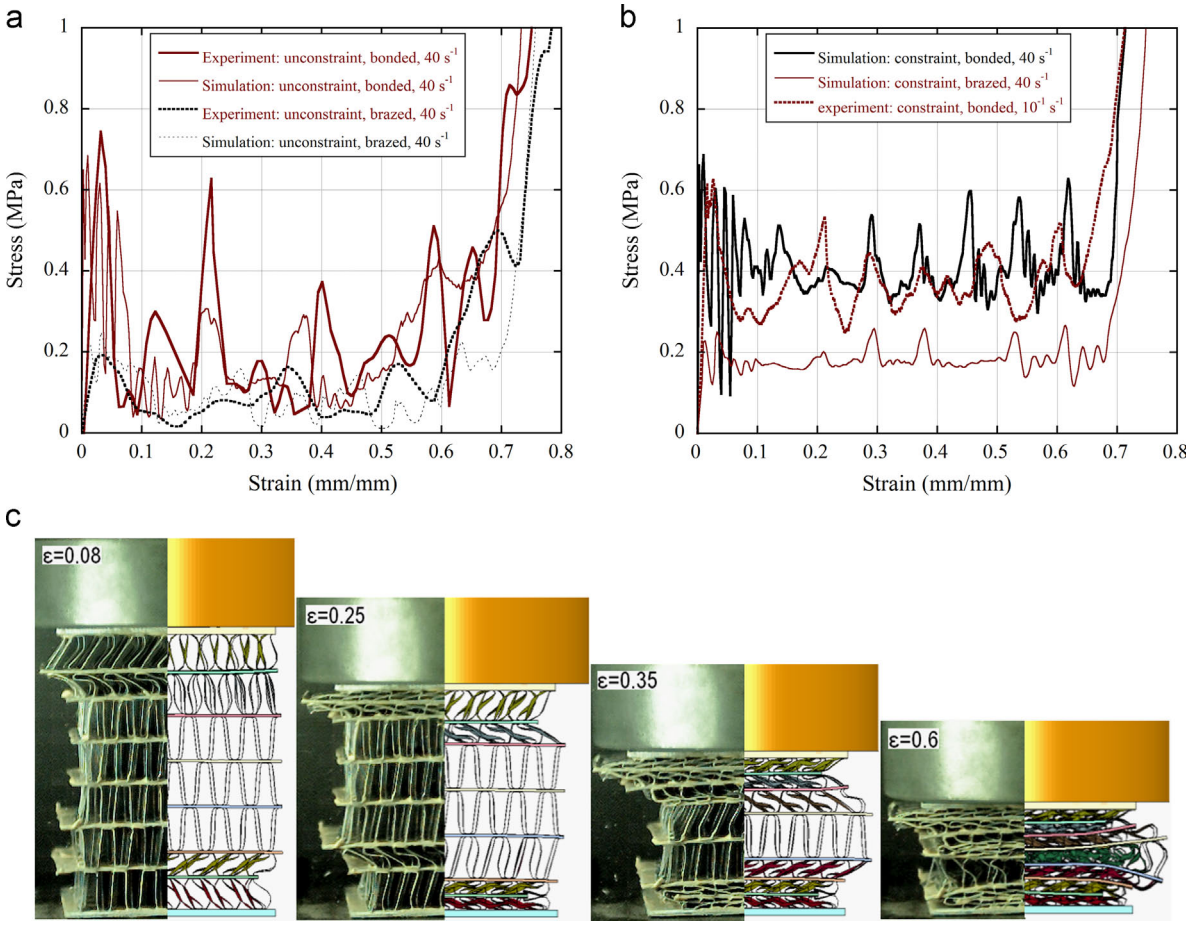

Fig. 11. Simulation and experimental stress–strain curves multi-layer sandwiches tested at 40 s^{-1}: (a) unconstraint and (b) constraint tests and (c) the experimental and simulation deformation pictures of bonded multi-layer samples.

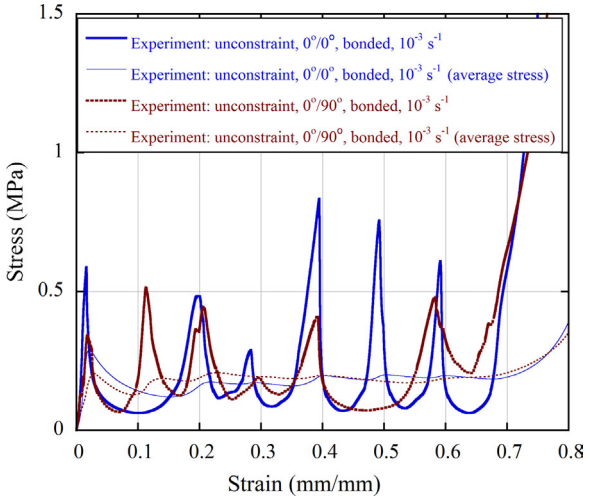

Fig. 12. Stress–strain curves of 0°/0° and 0°/90° core oriented multi-layer sandwich specimens tested at the strain rate of 10^{-3} s^{-1}.

localized type deformation in 0°/0° core oriented sample. This naturally decreases the post buckling stress values. The simulation buckling stress increases significantly at 40 s^{-1}, showing a high strain rate sensitive buckling stress; while the post buckling stress levels are not affected with increasing strain rate. The presence of interlayer sheets in 0°/0° core oriented sample is noted to induce relatively more stable and progressive collapse of the core layers. A completely different deformation mode is detected in 0°/90° core oriented multi-layer specimens, depicted in Fig. 13(b). In this orientation, the deformation is localized in individual core layers, which is very a similar deformation mode with that of multi-layer samples with interlayer sheets. A progressive deformation mode is clearly seen in both experiments and numerical simulations (Fig. 13(b)). Therefore, the stress values of 0°/90° core oriented multi-layer specimens are higher than those of 0°/0° core oriented multi-layer specimens without interlayer sheets. The simulation buckling stress at 40 s^{-1} and 10^{-1} s^{-1} are very much similar, showing a insignificant strain rate effect on the buckling stress in this direction.

The increased deformation forces at increasing strain rates in the compression of aluminum honeycomb structures through out of plane [33], metallic columnar structures [34], aluminum foams [33,35] and balsa wood in the axial direction [36,37] were reported to result from the micro-inertial effects. The inertia sensitive structures, classified as Type II structures by Calladine and English [38], are characterized with a strong softening behavior after yielding at quasi-static strain rates. The increased buckling stress of 0°/0° oriented core sandwich is due to micro-inertial effect. The lateral inertia forces lead to increased bending forces at increasing impact velocities.

The use of interlayer sheets is advantageous when the separation of corrugated layers is required or perquisite. The presence of interlayer sheets, which induces more homogenous and progressive deformation of the individual layers, increases the indentation resistance in the expense of reduced specific energy absorption as depicted in Fig. 14. The presence of interlayer sheets induced more homogenous and progressive deformation of individual layers in

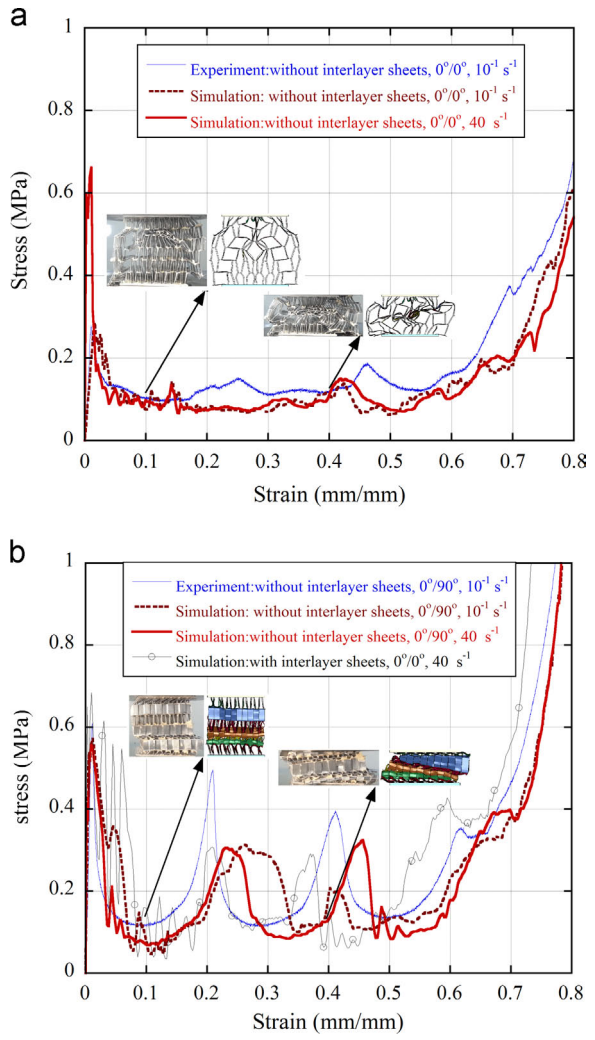

Fig. 13. The experimental and simulation stress–strain curves of (a) 0°/0° and (b) 0°/90° core orientated sandwiches without interlayer sheets.

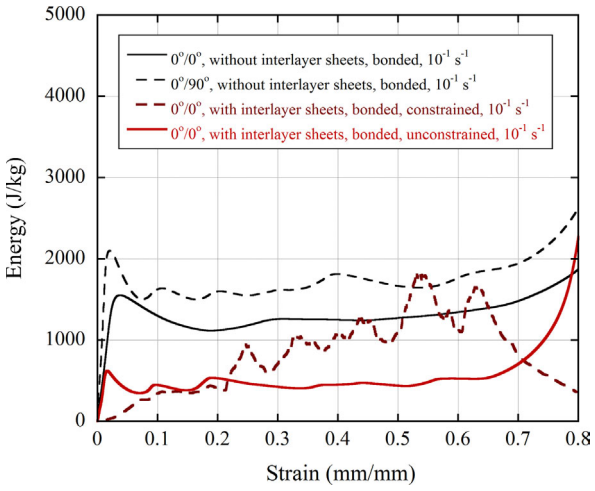

Fig. 14. Energy absorption vs. strain curves of multi-layer sandwich samples with and without interlayer sheet layers.

the expense of reduced specific energy absorption. This was due to the increase weight of the sandwiches with the inclusion of the interlayer sheets. A compromise between the interlayer sheet thickness and homogenous and progressive deformation of individual layers is therefore needed to increase the specific energy of the sandwiches with interlayer sheets. In the applications involving localized type of impact, the presence of interlayer sheets certainly increases the perforation resistance. The corrugated structures without interlayer sheets become advantageous when the impact pulse is distributed over a relatively larger area.

6. Conclusions

The axial crushing response of multi-layer, bonded and brazed, 1050 H14 trapezoidal aluminum corrugated core sandwich structures were investigated both experimentally and numerically at quasi-static and dynamic strain rates. Multi-layering decreased buckling stress and increased the densification strain of corrugated sandwich structure. The deformation modes of bonded and brazed samples were found to be similar; while, bonded specimens experienced higher crushing stresses, resulting from the reduced yield stresses of corrugated, interlayer and face sheets after brazing at elevated temperature. The simulation and experimental results were found to reasonably agree with each at the large extent of deformation and revealed the progressive fin folding of corrugated core layers and shearing the interlayer sheets as the main deformation modes. The unconstraint samples showed increased buckling stress at high strain rate, while constraint sample showed strain rate independent buckling stress. Both, the simulation and experimental post-bucking stresses increased with constraining. The multilayer samples in 0°/90° core orientation showed higher buckling stress than the samples in 0°/0° core orientation. The increased buckling stress of 0°/0° oriented core sandwiches was attributed to the micro-inertial effect which led to increased bending forces at increasing impact velocities. The presence of interlayer sheets induced more homogenous and progressive deformation of individual layers in the expense of reduced specific energy absorption.

Acknowledgments

The authors would like to thank Cumhur Akar for providing corrugated aluminum core samples.

References

[1] Compston P, Styles M, Kalyanasundaram S. Low energy impact damage modes in aluminum foam and polymer foam sandwich structures. J Sandw Struct Mater 2006;8:365–79.
[2] Hou WH, Zhu F, Lu GX, Fang DN. Ballistic impact experiments of metallic sandwich panels with aluminium foam core. Int J Impact Eng 2010;37:1045–55.
[3] Kiratisaevee H, Cantwell WJ. Low-velocity impact response of high-performance aluminum foam sandwich structures. J Reinf Plast Compos 2005;24:1057–72.
[4] Mohan K, Yip TH, Idapalapati S, Chen Z. Impact response of aluminum foam core sandwich structures. Mater Sci Eng A—Struct Mater Prop Microstruct Process 2011;529:94–101.
[5] Odaci IK, Kilicaslan C, Tasdemirci A, Guden M. Projectile impact testing of glass fiber-reinforced composite and layered corrugated aluminium and aluminium foam core sandwich panels: a comparative study. Int J Crashworthiness 2012;17:508–18.
[6] Pattofatto S, Zeng H, Zhao H. On the piercing force enhancement of aluminum foam sandwich plates under impact loading. J Sandw Struct Mater 2012;14:211–26.
[7] Sriram R, Vaidya UK, Kim JE. Blast impact response of aluminum foam sandwich composites. J Mater Sci 2006;41:4023–39.
[8] Zhao H, Elnasri I, Girard Y. Perforation of aluminium foam core sandwich panels under impact loading—an experimental study. Int J Impact Eng 2007;34:1246–57.
[9] Kiratisaevee H, Cantwell WJ. The impact response of aluminum foam sandwich structures based on a glass fiber-reinforced polypropylene fiber–metal laminate. Polym Compos 2004;25:499–509.

[10] Crupi V, Epasto G, Guglielmino E. Collapse modes in aluminium honeycomb sandwich panels under bending and impact loading. Int J Impact Eng 2012;43:6–15.
[11] Foo CC, Chai GB, Seah LK. Quasi-static and low-velocity impact failure of aluminium honeycomb sandwich panels. Proc Inst Mech Eng Part L—J Mater Des Appl 2006;220:53–66.
[12] Foo CC, Seah LK, Chai GB. Low-velocity impact failure of aluminium honeycomb sandwich panels. Compos Struct 2008;85:20–8.
[13] Francesconi A, Pavarin D, Bettella A, Giacomuzzo C, Faraud M, Destefanis R, et al. Generation of transient vibrations on aluminum honeycomb sandwich panels subjected to hypervelocity impacts. Int J Impact Eng 2008;35:1503–9.
[14] Hazizan MA, Cantwell WJ. The low velocity impact response of an aluminium honeycomb sandwich structure. Compos Part B—Eng 2003;34:679–87.
[15] Shitta-Bey OT, Carruthers JJ, Soutis C, Found MS. The localized low-velocity impact response of aluminium honeycombs and sandwich panels for occupant head protection: experimental characterization and analytical modelling. Int J Crashworthiness 2007;12:549–58.
[16] Radford DD, Fleck NA, Deshpande VS. The response of clamped sandwich beams subjected to shock loading. Int J Impact Eng 2006;32:968–87.
[17] Wadley HNG. Multifunctional periodic cellular metals. Philos Trans R Soc. A—Math Phys Eng Sci 2006;364:31–68.
[18] Liang C-C, Yang M-F, Wu P-W. Optimum design of metallic corrugated core sandwich panels subjected to blast loads. Ocean Eng 2001;28:825–61.
[19] Tilbrook MT, Radford DD, Deshpande VS, Fleck NA. Dynamic crushing of sandwich panels with prismatic lattice cores. Int J Solids Struct 2007;44:6101–23.
[20] Liang Y, Louca L, Hobbs R. Corrugated panels under dynamic loads. Int J Impact Eng 2007;34:1185–201.
[21] Zhang YC, Zhang SL, Wang ZL. Crush behavior of corrugated cores sandwich panels. In: Zhou M, editor. High performance structures and materials engineering, Pts 1 and 2. Stafa-Zurich: Trans Tech Publications Ltd.; 2011. p. 1584–9.
[22] Cote F, Deshpande V, Fleck N, Evans A. The compressive and shear responses of corrugated and diamond lattice materials. Int J Solids Struct 2006;43:6220–42.
[23] Rubino V, Deshpande V, Fleck N. The dynamic response of end-clamped sandwich beams with a Y-frame or corrugated core. Int J Impact Eng 2008;35:829–44.
[24] Rubino V, Deshpande VS, Fleck NA. The dynamic response of clamped rectangular Y-frame and corrugated core sandwich plates. Eur J Mech—A/Solids 2009;28:14–24.
[25] Lee S, Barthelat F, Hutchinson JW, Espinosa HD. Dynamic failure of metallic pyramidal truss core materials—experiments and modeling. Int J Plast 2006;22:2118–45.
[26] Yungwirth CJ, Wadley HNG, O'Connor JH, Zakraysek AJ, Deshpande VS. Impact response of sandwich plates with a pyramidal lattice core. Int J Impact Eng 2008;35:920–36.
[27] Kilicaslan C, Guden M, Odaci IK, Tasdemirci A. The impact responses and the finite element modeling of layered trapezoidal corrugated aluminum core and aluminum sheet interlayer sandwich structures. Mater Des 2013;46:121–33.
[28] ASTM Standard E 8M-04. Standard specification for standard test methods for tension testing of metallic materials. West Conshohocken, PA: ASTM International; 2004 ⟨www.astm.org.in⟩.
[29] LSTC. LS-DYNA keyword user's manual. Livermore Software Technology Corporation (LSTC); 2007.
[30] Gumruk R, Karadeniz S. A numerical study of the influence of bump type triggers on the axial crushing of top hat thin-walled sections. Thin-Walled Struct 2008;46:1094–106.
[31] Johnson W, Mamalis AG. A survey of some physical defects arising in metal working processes. In: Proceedings of the 17th international MTDR conference. London, UK; 1977. p. 607–21.
[32] Gibson LJ. Mechanical behavior of metallic foams. Annu Rev Mater Sci 2000;30:191–227.
[33] Zhao H, Elnasri I, Abdennadher S. An experimental study on the behaviour under impact loading of metallic cellular materials. Int J Mech Sci 2005;47:757–74.
[34] Langseth M, Hopperstad OS. Static and dynamic axial crushing of square thin-walled aluminium extrusions. Int J Impact Eng 1996;18:949–68.
[35] Paul A, Ramamurty U. Strain rate sensitivity of a closed-cell aluminum foam. Mater Sci Eng A 2000;281:1–7.
[36] Reid SR, Peng C. Dynamic uniaxial crushing of wood. Int J Impact Eng 1997;19:531–70.
[37] Tagarielli VL, Deshpande VS, Fleck NA. The high strain rate response of PVC foams and end-grain balsa wood. Compos Part B: Eng 2008;39:83–91.
[38] Calladine CR, English RW. Strain-rate and inertia effects in the collapse of two types of energy-absorbing structure. Int J Mech Sci 1984;26:689–701.